Solution structure of the C-terminal X domain of the measles virus phosphoprotein and interaction with the intrinsically disordered C-terminal domain of the nucleoprotein

ARTICLE *in* JOURNAL OF MOLECULAR RECOGNITION · SEPTEMBER 2010

Impact Factor: 2.15 · DOI: 10.1002/jmr.1010 · Source: PubMed

Research Article

Journal of Molecular Recognition

Received: 7 September 2009, Revised: 4 November 2009, Accepted: 5 November 2009, Published online in Wiley InterScience: 2010

(www.interscience.wiley.com) DOI:10.1002/jmr.1010

Solution structure of the C-terminal X domain of the measles virus phosphoprotein and interaction with the intrinsically disordered C-terminal domain of the nucleoprotein

Stéphane Gely[a†], David F. Lowry[b†], Cédric Bernard[a], Malene R. Jensen[c], Martin Blackledge[c], Stéphanie Costanzo[a], Jean-Marie Bourhis[a‡], Hervé Darbon[a], Gary Daughdrill[b] and Sonia Longhi[a]***

In this report, the solution structure of the nucleocapsid-binding domain of the measles virus phosphoprotein (XD, aa 459–507) is described. A dynamic description of the interaction between XD and the disordered C-terminal domain of the nucleocapsid protein, (N_{TAIL}, aa 401–525), is also presented. XD is an all α protein consisting of a three-helix bundle with an up-down-up arrangement of the helices. The solution structure of XD is very similar to the crystal structures of both the free and bound form of XD. One exception is the presence of a highly dynamic loop encompassing XD residues 489–491, which is involved in the embedding of the α-helical XD-binding region of N_{TAIL}. Secondary chemical shift values for full-length N_{TAIL} were used to define the precise boundaries of a transient helical segment that coincides with the XD-binding domain, thus shedding light on the pre-recognition state of N_{TAIL}. Titration experiments with unlabeled XD showed that the transient α-helical conformation of N_{TAIL} is stabilized upon binding. Lineshape analysis of NMR resonances revealed that residues 483–506 of N_{TAIL} are in intermediate exchange with XD, while the 475–482 and 507–525 regions are in fast exchange. The N_{TAIL} resonance behavior in the titration experiments is consistent with a complex binding model with more than two states. Copyright © 2010 John Wiley & Sons, Ltd.

Supporting information may be found in the online version of this paper.

Keywords: measles virus; nucleoprotein; phosphoprotein; solution structure; NMR spectral assignment; intrinsic disorder; induced folding; disorder-to-order transitions; residual structure; conformer selection

INTRODUCTION

Measles virus (MeV), a member of the *Paramyxoviridae* family, possesses a non-segmented negative-sense, single-stranded RNA genome that is encapsidated by the nucleoprotein (N) within a helical nucleocapsid. Transcription and replication of the MeV genome is controlled by the viral RNA-dependent RNA polymerase (RdRp) (Longhi and Canard, 1999). The RdRp is a complex consisting of a catalytic subunit (L) and the phosphoprotein (P), with P serving as an essential polymerase co-factor

* *Correspondence to: S. Longhi, Architecture et Fonction des Macromolécules Biologiques (AFMB) UMR 6098, CNRS and Universités d'Aix-Marseille I and II 163, Avenue de Luminy, Case 932, 13288 Marseille Cedex 09, France. E-mail: Sonia.Longhi@afmb.univ-mrs.fr*

** *Correspondence to: G. Daughdrill, Center for Biomolecular Identification and Targeted Therapeutics, University of South Florida, 3720 Spectrum Blvd., Tampa, FL 33612, USA E-mail: gdaughdr@cas.usf.edu*

a *S. Gely, C. Bernard, S. Costanzo, J.-M. Bourhis, H. Darbon, S. Longhi Architecture et Fonction des Macromolécules Biologiques (AFMB), UMR 6098, CNRS, France and Universités d'Aix-Marseille I and II, 163 avenue de Luminy, 13288 Marseille Cedex 09, France*

b *D. F. Lowry, G. Daughdrill Department of Cell Biology, Microbiology, and Molecular Biology, and the Center for Biomolecular Identification and Targeted Therapeutics, University of South Florida, 3720 Spectrum Blvd. Tampa, FL 33612, USA*

c *M. R. Jensen, M. Blackledge Protein Dynamics and Flexibility, Institut de Biologie Structurale Jean-Pierre Ebel, UMR 5075, CEA-CNRS-UJF, 41 Rue Jules Horowitz, 38027 Grenoble, France*

† *These authors contributed equally to the work.*

‡ *Present address: IBCP UMR 5086 CNRS, 7, passage du Vercors 69367 Lyon, Cedex 07, France.*

Abbreviations: *HSQC, heteronuclear single quantum correlation; IDP, intrinsically disordered protein; IPTG, isopropyl ß-D-thiogalactopyranoside; L, large protein; MeV, measles virus; MoRE, Molecular Recognition Element; MuV, mumps virus; N, nucleoprotein; NMR, nuclear magnetic resonance; P, phosphoprotein; PMSF, phenyl-methyl-sulfonyl-fluoride; RMSD, root mean square deviation; SAXS, small-angle X-ray scattering; SeV, Sendai virus; XD, X domain of P.*

that recruits the L protein onto the nucleocapsid template (Figure 1A). P is a modular protein consisting of alternating disordered and ordered regions (Karlin *et al.*, 2002a; Karlin *et al.*, 2003) (Figure 1A). The MeV nucleoprotein (N) is also composed of an ordered and disordered region: an ordered N-terminal domain, N_{CORE} (N^{1-400}), which contains all the regions necessary for self-assembly and RNA-binding (Karlin *et al.*, 2002b), and a disordered C-terminal domain N_{TAIL} ($N^{401-525}$) (Longhi *et al.*, 2003) that is exposed at the surface of the viral nucleocapsid and serves as a tethering anchor for the P–L polymerase complex (Figure 1A). The nucleocapsid-binding domain of P has been mapped to the C-terminal X domain ($P^{459-507}$) (Johansson *et al.*, 2003; Kingston *et al.*, 2004b) and its crystal structure has been solved at 1.8 Å resolution (Johansson *et al.*, 2003) (Figure 1A). XD has been shown to induce α-helical folding of N_{TAIL}(Johansson *et al.*, 2003), with a conserved region of N_{TAIL} (Box2, aa 489–506) being required for this structural transition (Bourhis *et al.*, 2004; Bourhis *et al.*, 2005a) (for reviews see Bourhis *et al.*, 2005b; Bourhis *et al.*, 2006; Bourhis and Longhi, 2007; Longhi, 2009). Using computational approaches, Box2 was shown to possess an α-More (aa 489–499) (Figure 1A), where MoREs (Molecular Recognition Elements) are interaction-prone short segments that

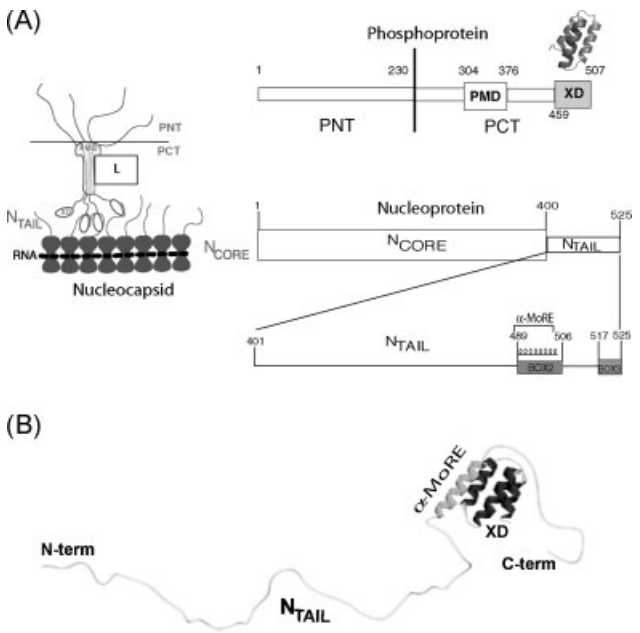

Figure 1. (A) Schematic representation of the polymerase complex (L–P) bound to the nucleocapsid template (left) and modular organization of the P and N protein, where globular and disordered regions are represented by large and narrow boxes, respectively (right). The disordered N_{TAIL} ($N^{401-525}$) and PNT (P^{1-230}) regions are represented by lines. The encapsidated RNA is shown as a dotted line embedded in the middle of N (Albertini *et al.*, 2006) and (Green *et al.*, 2006). The multimerization domain of P ($P^{304-375}$, PMD) is represented with a dumbbell shape by analogy with the SeV PMD structure (Tarbouriech *et al.*, 2000). The segment connecting PMD and XD is represented as disordered according to (Longhi *et al.*, 2003) and (Karlin *et al.*, 2003). The L protein is shown as a rectangle contacting P through PMD. The crystal structure of XD (pdb code 1OKS) is also shown. (B) Model of the N_{TAIL}–XD complex as derived by SAXS studies (Bourhis *et al.*, 2005a). The structure of the chimera between XD and the N_{TAIL} region encompassing residues 486–504 (pdb code 1T60) is shown. Structures were drawn using Pymol (DeLano, 2002).

become ordered (i.e. more rigid) upon specific binding (Oldfield *et al.*, 2005; Mohan *et al.*, 2006; Fuxreiter *et al.*, 2007; Vacic *et al.*, 2007).

Structural data available so far for the N_{TAIL}-XD complex arise from crystallographic studies of a chimeric construct consisting of XD and of the 486–504 region of N_{TAIL} (Kingston *et al.*, 2004a), and from small angle X-ray scattering (SAXS) studies of the complex between XD and the entire N_{TAIL} domain (Bourhis *et al.*, 2005a). Crystallographic studies showed that the α-MoRE is embedded in a hydrophobic cleft delimited by helices α2 and α3 of XD to form a pseudo-four helix arrangement (Kingston *et al.*, 2004a). The low-resolution, SAXS-derived model of the complex (Figure 1B), revealed that most of N_{TAIL} ($N^{401-488}$) remains disordered in the complex and does not establish contacts with XD, contrary to the α-MoRE (Figure 1). On the other hand, the lack of a flexible appendage emerging from the globular part of the model, which accommodates XD and the α-MoRE, suggested that the C-terminal region of N_{TAIL} might also contribute to the interaction with XD (see Figure 2 in Bourhis *et al.*, 2005a). That the C-terminal Box3 ($N^{517-525}$) region does contribute to binding to XD has been further confirmed by surface plasmon resonance studies, where removal of this region caused the dissociation constant of the XD-binding reaction to increase from 80 nM (for full-length N_{TAIL}) to 120 μM (Bourhis *et al.*, 2005a). We recently reported two EPR spectroscopy studies, where we targeted 14 sites scattered within N_{TAIL} for site-directed spin-labeling, with 12 of them being located within the reported region of interaction with XD (Morin *et al.*, 2006; Belle *et al.*, 2008). By means of a thorough analysis of spin label mobility under various conditions, we showed that the 488–502 region is more rigid than the rest of the protein, consistent with the existence of a transiently populated α-helix. Upon binding to XD, this region experiences a dramatic gain of rigidity, while the 505–522 region is only moderately affected by XD. In addition, we showed that XD triggers α-helical folding of the 488–502 region only, while the downstream region does not become helical, nor does it establish direct contacts with XD. Lack of direct contacts between Box3 and XD, has been indeed recently confirmed by heteronuclear single quantum correlation (HSQC) experiments, where no chemical shift variation was obtained upon addition of an unlabeled Box3 peptide to ^{15}N-labeled XD (Bernard *et al.*, 2009).

Based on all these data, we have proposed a model where the N_{TAIL}–XD interaction would rely on a "folding-before-binding" mechanism, involving recognition by XD of the transiently pre-structured α-MoRE in the unbound form. It was also postulated that the region downstream of the α-MoRE would act (i) either by stabilizing the α-helical conformation of Box2 through the establishment of transient tertiary contacts (ii) or by stabilizing the N_{TAIL}–XD complex through a reduction of the entropic penalty in the binding process arising from the persistence of the flexible (e.g. disordered) nature of this region even upon complex formation (Belle *et al.*, 2008; Bernard *et al.*, 2009).

High-resolution structural data are also available for the X domains of the closely related mumps and Sendai viruses (MuV and SeV), the structure of which has been solved by X-ray crystallography and NMR, respectively (Blanchard *et al.*, 2004; Kingston *et al.*, 2008). The MuV X domain ($P^{343-391}$) has a few notable distinguishing properties with respect to MeV and SeV XD. Indeed, MuV XD has been shown to exist as a molten globule, being loosely packed and devoid of stable tertiary structure (Kingston *et al.*, 2004b; Kingston *et al.*, 2008). In addition, contrary to the MeV and SeV X domains, MuV XD does not interact with N_{TAIL} and rather

establish contacts with the structured N_{CORE} region of N (Kingston *et al*., 2004b).

In the case of SeV, NMR studies have also been carried out on the 474–568 region of P (referred to as PX), which beyond the structured C-terminal X domain ($P^{516–568}$) also contains a disordered domain ($P^{474–515}$) (Bernado *et al*., 2005; Houben *et al*., 2007b). The X domains of the three viruses share the same overall architecture, consisting of a triple α-helical bundle. Although in both MeV and SeV, the N_{TAIL}–XD interaction has been shown to lead to α-helical folding of N_{TAIL} (Johansson *et al*., 2003; Bourhis *et al*., 2004; Bourhis *et al*., 2005a; Houben *et al*., 2007a), a few features distinguish the SeV N_{TAIL}–XD complex from the MeV one. In particular, in SeV N_{TAIL} the XD binding region is restricted to a region with α-helical propensities ($N^{472–493}$), while the C-terminus is not involved in the interaction (Houben *et al*., 2007a). Secondly, while binding between MeV XD and MeV N_{TAIL} occurs with a rather strong affinity ($K_D = 80$ nM) (Bourhis *et al*., 2005a), the experimentally determined K_D for the SeV couple is much higher (60 μM)(Houben *et al*., 2007a). Finally, contrary to the MeV N_{TAIL}–XD complex that is mediated by hydrophobic interactions (Johansson *et al*., 2003; Kingston *et al*., 2004a), the SeV binding interface is dominated by charged residues (Houben *et al*., 2007a).

Using an original approach for characterizing complex multi-conformational equilibria from experimentally measured residual dipolar couplings, the level and nature of helical sampling present in SeV N_{TAIL} has been quantitatively analyzed. These studies showed that the molecular recognition element of the SeV N_{TAIL} domain preferentially populates three specific overlapping helical conformers. These studies also showed that the unfolded N_{TAIL} regions adjacent to the helix are projected in the direction of XD, identifying a mechanism by which they could achieve non-specific encounter interactions prior to binding to the partner (Jensen *et al*., 2008).

Although the MeV N_{TAIL}–XD interaction has been the focus of numerous studies, only partial structural information on the N_{TAIL}–XD complex is presently available. Indeed, crystallographic data have been obtained on a chimeric construct containing only 18 out of 125 N_{TAIL} residues (Kingston *et al*., 2004a), and NMR studies carried out with the entire N_{TAIL} domain and XD did not provide full structural information because of the lack of assignment of the N_{TAIL} HSQC spectrum (Bourhis *et al*., 2005a). On the other hand, SAXS data (Bourhis *et al*., 2005a) only provided global low-resolution structural information. Consequently, the actual conformation of the region downstream the α-MoRE in the complex is not known, nor is the structural description of the free form of N_{TAIL} available. In particular, quantitative information on the extent of α-helical sampling of the α-MoRE in the absence of the partner is lacking.

In order to achieve a description of the conformation of MeV XD and N_{TAIL} in solution, and as a first step towards the determination of the solution structure of XD in complex with the interacting N_{TAIL} region, we herein report the determination of the NMR solution structure of XD, as well as the resonance assignments of the disordered N_{TAIL} domain in both the free and bound form.

MATERIALS AND METHODS

XD and N_{TAIL} samples preparation

Expression and purification of unlabeled XD, encompassing residues 459–507 of P (strain Edmonston B) and bearing a C-terminal hexahistidine-tag, were carried out as already described (Johansson *et al*., 2003). The N_{TAIL} construct, encoding residues 401–525 of N (strain Edmonston B) and bearing an N-terminal hexahistidine tag has already been described (Bourhis *et al*., 2005a).

Isotopically labeled (^{15}N) XD and (^{13}C,^{15}N) or (^{15}N) N_{TAIL} samples were prepared by growing transformed Rosetta pLysS (Stratagene) bacteria in minimal M9 medium supplemented with either $^{15}NH_4Cl$ (1 g/L) *plus* ^{13}C-glucose (2 g/L) or $^{15}NH_4Cl$ (1 g/L) *plus* glucose (2 g/L). A 150 ml preculture grown overnight to saturation in LB medium containing 100 μg/ml ampicillin and 17 μg/ml chloramphenicol was harvested, washed in minimal M9 medium, and inoculated into 1 L of minimal M9 medium supplemented with ampicillin and chloramphenicol. The culture was grown at 37°C. At an OD_{600} of 0.5, IPTG was added to a final concentration of 0.2 mM and the cells were grown over night at 28°C. The induced cells were harvested, washed, and collected by centrifugation. The resulting pellets were frozen at −20°C. Prior to lysis, they were resuspended in five volumes (v/w) buffer A (50 mM sodium phosphate pH 7, 300 mM NaCl, 10 mM Imidazole, 0,02% NaN_3, 1 mM phenyl-methyl-sulfonyl-fluoride (PMSF) supplemented with 0.1 mg/ml lysozyme, 10 μg/ml DNAse I, and protease inhibitor cocktail (Sigma) (1 ml per 25 ml of bacterial lysate). After a 20 min incubation with gentle agitation, the cells were disrupted by sonication (using a 750 W sonicator and four cycles of 30 s each at 60% power output). The lysates were clarified by centrifugation at 30 000 g for 30 min. Starting from a 1 L culture, the clarified supernatant was incubated for 1 h with gentle shaking with 4 ml Chelating Sepharose Fast Flow Resin preloaded with Ni^{2+} (N_{TAIL}) or Co^{2+} (XD) ions (GE, Healthcare), previously equilibrated in buffer A. The resin was washed with buffer A, and the N_{TAIL} protein was eluted in buffer A containing 250 mM imidazole. Eluates were analyzed by SDS-PAGE for the presence of the desired product. The fractions containing the protein were pooled and further purified by gel filtration. In the case of N_{TAIL}, a protease inhibitor cocktail (Sigma) was added (1 μl per ml of protein solution) prior to loading onto a Superdex 75 HR 16/60 column (GE, Healthcare). Elution was carried out with either buffer B (50 mM sodium phosphate pH 7, 50 mM NaCl, 1 mM EDTA, 0.02% NaN_3) (^{15}N labeled N_{TAIL} and unlabeled XD samples) or 10 mM sodium phosphate pH 8 (^{15}N labeled XD). The fractions containing the protein of interest were pooled, concentrated using Centricon Plus-20 (molecular cutoff: 3000 Da) (Millipore) and then stored at −20°C.

All purification steps, except for gel filtrations, were carried out at 4°C. Apparent molecular mass of proteins eluted from gel filtration columns was deduced from a calibration carried out with LMW and HMW calibration kits (GE, Healthcare).

NMR data collection and spectra analysis

XD ^1H spectra were recorded at 300 K on a Bruker DRX 500 MHz spectrometer equipped with an HCN probe. Spectra were processed with XWinNMR version 2.1 and analyzed with NMRView 1.2. (Johnson and Blevins, 1994). An XD sample at 1.6 mM in a 10 mM sodium phosphate pH 8 buffer containing 10% D_2O was used. Since the sequential assignment of XD was already known (Bernard *et al*., 2009), structure calculation only required a 2D NOESY (Macura and Ernst, 1980) spectrum that was recorded with a mixing time of 100 ms. Heteronuclear NOEs were determined as described previously (Farrow *et al*., 1994).

N_{TAIL} spectra were recorded at a temperature of 298 K on a Varian Inova spectrometer equipped with a cold probe operating at a ^{1}H resonance frequency of 600 MHz. The resonance assignment of N_{TAIL} was obtained using a double-labeled ($^{15}N/^{13}C$) sample at a concentration of either 0.5 or 0.8 mM in a buffer containing 10% D_2O, 50 mM sodium phosphate pH 6.5, 50 mM NaCl, 1 mM EDTA, and 0.02% NaN_3 (buffer C). ^{1}H and ^{15}N, as well as $^{13}C\alpha$, $^{13}C_{\beta}$, and $^{13}C'$ assignments were obtained from a series of BEST-type triple resonance experiments: HNCO, intra-residue HN(CA)CO, HN(CO)CA, intra-residue HNCA, HN(CO-CA)CB, and intra-residue HN(CA)CB (Schanda *et al*., 2006; Lescop *et al*., 2007). All triple resonance experiments were acquired with a sweep width of 7.5 kHz and 512 complex points in the ^{1}H dimension and a sweep width of 1.3 kHz and 32 complex points in the ^{15}N dimension. For the ^{13}C dimension, the spectra were acquired with a sweep width of 1.7 kHz and 60 complex points (HNCO and intra-residue HN(CA)CO), 3 kHz and 110 complex points (HN(CO)CA and intra-residue HNCA), and 9.5 kHz and 100 complex points (HN(COCA)CB and intra-residue HN(CA)CB).

Spectra were processed in NMRPipe (Delaglio *et al*., 1995) and analyzed using Sparky (Goddard and Kneller, 2003). The program Mars (Jung and Zweckstetter, 2004) was used for automatic assignment of spin systems.

Sensitivity enhanced HNCACB, CBCACONH, and HNCO experiments (Kay *et al*., 1992; Wittekind and Mueller, 1993; Muhandiram and Kay, 1994) were performed on the N_{TAIL}-XD complex on a 0.8 mM double-labeled ($^{15}N/^{13}C$) sample of N_{TAIL} in buffer C following the addition of an equimolar amount of unlabeled XD in buffer B. Addition of XD at ratios greater than 1:1 resulted in precipitation. HNCACB and CBCACONH experiments were acquired using a sweep width of 8000 Hz and 512 complex t3 points in the ^{1}H dimension, a sweep width of 12065.5 Hz and 128 complex t1 points in the ^{13}C dimension, and a sweep width of 1400 Hz and 32 complex t2 points in the ^{15}N dimension. For the HNCO experiments, parameters were identical to the HNCACB for the ^{1}H and ^{15}N dimensions. HNCO experiments were acquired using a sweep width of 3017.1 Hz and 64 complex t1 points in the ^{13}C dimension. Besides standard triple resonances experiments, for bound resonances that did not disappear during the course of the titration, assignments were made based on inference using the criterion of a minimal perturbation in the spectra from one titration point to the next.

Quantitative analysis of NMR titration data was performed as described by (Bernard *et al*., 2009). The dissociation constant K_D can be estimated from the changes in chemical shifts of the ^{15}N-labeled protein (P) caused by addition of the unlabeled binding partner (L), by fitting the chemical shift changes to the following equation for a two-state model in fast exchange:

$$\Delta\delta_{ppm} = \frac{\Delta\delta_{MAX}}{2[L]}\left([P] + [L] + K_D - \sqrt{([P] + [L] + K_D)^2 - 4[P][L]}\right) \quad (1)$$

where $\Delta\delta_{ppm}$ is the combined chemical shift variation (in Hz), $\Delta\delta_{MAX}$ is the maximum chemical shift deviation between the free and the bound state of protein (P), and $[P]$ and $[L]$ are the total protein and ligand concentrations. The combined chemical shift variation is defined as $\Delta\delta_{ppm} = [\Delta\delta_{HN}^2 + (\Delta\delta_N/\text{Rscale})^2]^{1/2}$ (Mulder *et al*., 1999).

Curve fitting over experimental data was performed by using the XCRVFIT program (R. Boyko and B. D. Sykes, University of Alberta, Edmonton, Alberta, Canada).

XD structure calculation

Initial structure calculations involved eight iterations on an extended input structure, using CNS protocols in ARIA software 1.2 (Linge *et al*., 2003), in which each iteration consisted of an automatic ambiguous Nuclear Overhauser Effect (NOE) assignment and calibration of the NOE distance restraints, followed by a simulated annealing procedure. In later stages of the ARIA calculations, hydrogen bond restraints were added. In each iteration, 200 XD structures were calculated, and the 40 ones with the lowest energy term were used in the next step. Prior to water refinement with the CNS protocol, a 10 000-step simulated annealing calculation using torsion angle dynamics was used in ARIA. Finally, the 20 structures with the lowest energy were selected as the ensemble to be analyzed and the geometric quality of the obtained structures was assessed by the PROCHECK-NMR software (Laskowski *et al*., 1993). Structural alignments amongst the various XD structures and calculations of root mean square deviation (RMSD) were performed using the McLachlan algorithm as implemented in the ProFit program (Martin, A.C.R. and Porter, C.T, http://www.bioinf.org.uk/software/profit/). Atomic coordinates have been deposited in the Protein Data Bank under accession code 2K9D. Chemical shifts have been deposited in the Biological Magnetic Resonance Data Bank under accession number 16000.

Note that hydrogen/deuterium exchange experiments could not be carried out as our attempts to lyophilize the sample were unsuccessful.

RESULTS

XD NMR resonance assignment and structure calculation

The sequential assignment procedure allowed us to determine the resonance frequency of almost all protons. The first three ($P^{459-461}$) and the last two ($P^{506-507}$) XD residues were not detected in the HSQC spectra and remained unassigned.

The structure of XD was determined by using 439 NOE-based distance restraints (including 215 intra-residue, 127 sequential, 70 medium-range, and 27 long-range). From preliminary structures obtained in the first iteration of ARIA we added 32 theoretical hydrogen bonds restraints that correspond to the three α-helices clearly identified by their characteristic NOE pattern. Altogether, the final experimental set corresponds to 10 constraints per residue on average. The best-fit superposition of backbone atoms for the 20 solution structures is shown in Figure 2. All the structures have good non-bonded contacts and good covalent geometry as evidenced by low values of energy terms and low RMSD values for bond lengths, valence angles and improper dihedral angles, with no distance violations greater than 0.5 Å. A summary of the structural statistics and the values of calculated RMSDs, is provided in Table 1.

Description of the XD solution structure and comparison with other closely-related XD structures

The 3D solution structure of XD consists of a monomeric, all α protein, built up by three helices encompassing residues 462–470, 475–487, and 492–505, respectively (see Figures 2 and 3). The topology of the protein is an up-down-up arrangement. The core of the protein is rich in non-polar amino acids that establish hydrophobic contacts and significantly

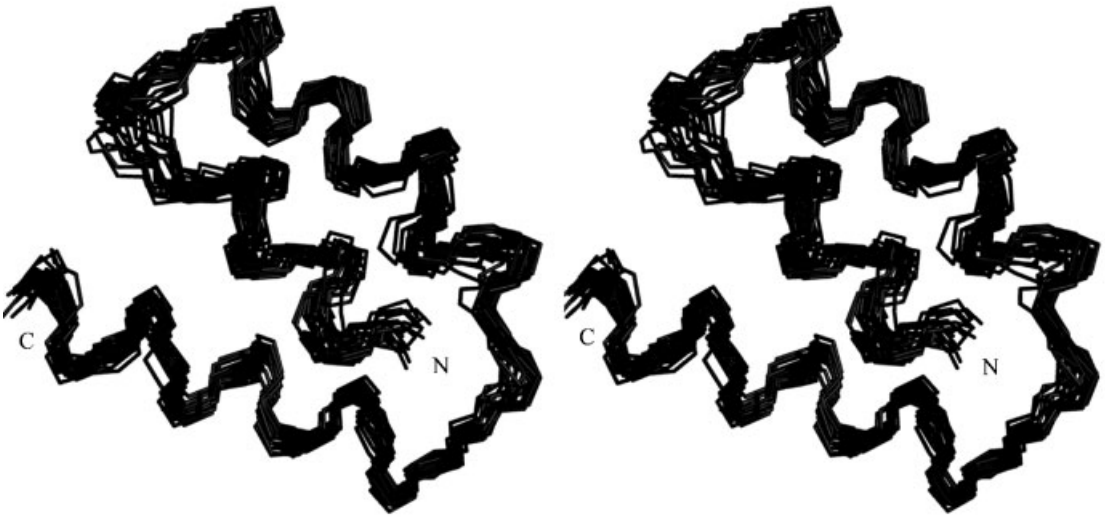

Figure 2. Stereo view of the superimposition of the 20 best solution structures of XD. The picture was drawn using Pymol (DeLano, 2002).

stabilize the 3D structure. The turn linking helix α1 to α2 and the one consisting of residues 488–491 exhibits low precision, as judged based on the scarcity of NOE for those residues. Heteronuclear NOE experiments showed that the structure is rigid with the exception of residues belonging to the turn linking the two last α–helices of the protein (residues 489–491) that exhibit a higher flexibility than the other residues as illustrated by their lower value of heteronuclear NOE (Figure 3). The negative heteronuclear NOE peak of residue Ala491, is indicative of a very flexible behavior, consistent with the small nature of the side-chain of this residue as well as with the presence of a Gly at position 490.

Table 1. Structure statistics for the 20 lowest energy XD structures

Average RMSDs to the mean structure (Å)	residues 462 to 505
Backbone	1.07
Heavy atoms	2.05
Energies (kcal/mol)	
Bond	11.11
Angle	66.87
Improper	120.6
van der Waals	−429.18
NOE[a]	21.18
Total	−209.42
RMSDs from ideal geometry	
Bond (A)	3.70E-03
Angle (°)	0.55
Improper (°)	1.45
Dihedral (°)	40.86
NOE (A)	2.90E-02
Ramachandran plot[b] (%)	
Most favored and additional allowed	98.8 +/−6.2
Generously allowed	0.5 +/−0.26
Disallowed regions	0.7 +/−0.32
Z-score	
Ramachandran plot appearance	0.019
Backbone conformation	−0.891
chi1/chi2 rotamer normality	−0.045

[a] No violation of the NOE-derived constraints larger than 0.5 Å is observed in any of the 20 structures.
[b] Calculated for the 20 structures using PROCHECK-NMR.

As already mentioned, two crystal structures of MeV XD are available: the free form (XD_{free}, pdb code 1OKS) (Johansson *et al*., 2003) and the structure of XD bound to the N_{TAIL} region encompassing residues 486–504 (XD_{bound}, pdb code 1T6O) (Kingston *et al*., 2004a). The secondary structure elements of the solution structure of XD (XD_{NMR}) superimpose well onto those of both crystal structures with an RMSD of 1.33 Å and of 1.38 Å for XD_{free} and XD_{bound}, respectively. Despite this overall similarity, some minor differences could be appreciated between the solution and crystal structures of XD (Figure 4A and data not shown). The helix α1 of XD_{NMR} is slightly closer to helices α2 and α3 than in the two crystal structures, and the last helix turn has a slightly different orientation with respect to the corresponding one in both crystal structures. This difference is very likely to be ascribed to the lack of restraints for the last two residues ($P^{506–507}$) in the calculation of XD_{NMR}. The main difference between the solution and crystal structures of XD concerns the turn (residues 489–491) that displays a high mobility in XD_{NMR}. Note that this turn accommodates two XD residues, namely K489 and G490, that undergo a profound chemical shift perturbation upon addition of unlabeled N_{TAIL}, being displaced from their original position following an intermediate exchange regime (Bernard *et al*., 2009).

Finally, we compared the solution structure of MeV XD to the structures of both SeV and MuV XD. The secondary structure elements of the three structures well superimpose onto each others (Figure 4B and data not shown), with RMSD values of 1.85 Å (SeV) and of 1.49 Å (MuV). The main difference between the MeV and the SeV XD solution structure resides in the more hydrophobic nature of the N_{TAIL} binding surface of the former (*cfr* Figures 4C and 4D).

N_{TAIL} NMR resonance assignment

The amide ^{1}H, ^{15}N, $^{13}C\alpha$, $^{13}C_{\beta}$, and $^{13}C'$ resonance assignments for N_{TAIL} and the N_{TAIL}–XD complex are provided as a supplemental

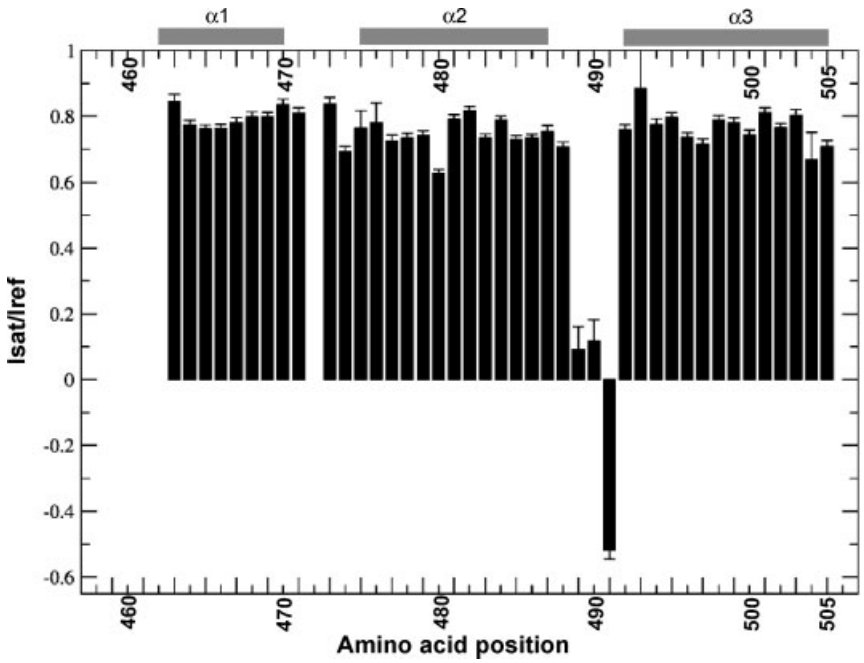

Figure 3. Backbone heteronuclear ^{1}H-^{15}N NOE represented as a function of P positions, where XD encompasses residues 459–507 of P. Values were calculated as I_{sat}/I_0 where I_{sat} and I_0 are the cross-peak intensity in the presence and in the absence of proton saturation, respectively. Blank slot indicate either overlapping or unassigned residues. Gray bars above the graph designate α-helices.

table (supplementary Table S1). 113 out of 118 non-proline, amide ^{1}H, ^{15}N, $^{13}C\alpha$, $^{13}C_{\beta}$, and $^{13}C'$ resonances were assigned in N_{TAIL}. In addition, the assignment of $^{13}C\alpha$, $^{13}C_{\beta}$, and $^{13}C'$ resonances of the seven proline residues was obtained. The ^{1}H and ^{15}N nuclei for residues T401, K435, Q442, S443, and R444 were not assigned, probably due to fast hydrogen exchange at this pH.

Intermediate exchange between N_{TAIL} and XD, especially at the binding interface, caused significant peak broadening thus reducing the number of resonance assignments possible for the

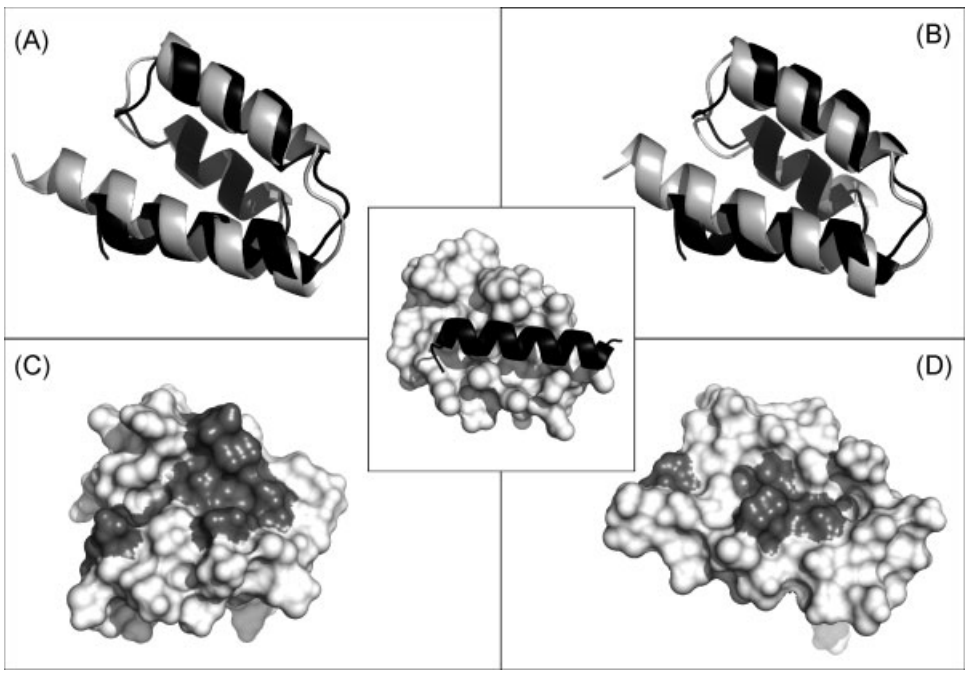

Figure 4. Structure comparison among available XD structures. (A, B) Superimposition of the average NMR structure of MeV XD (XD_{NMR}) onto (A) the crystal structure of MeV XD (XD_{free}) or (B) the NMR structure of SeV XD. The XD_{NMR} structure is drawn in black, while the other two structures are drawn in gray. (C, D) Molecular surface of MeV XD_{NMR} (C) and SeV XD (D). The hydrophobic residues within the N_{TAIL} binding surface of XD are highlighted in gray. The central inset shows the crystal structure of the chimeric construct encompassing XD (surface representation, white) and the N_{TAIL} region undergoing α-helical folding (residues 486–504 of N) (ribbon representation, black) (pdb code 1T6O). The pictures were drawn using Pymol (DeLano, 2002).

N_{TAIL}–XD complex. For the bound form of N_{TAIL}, 105 out of 118 non-proline, amide ^{1}H, ^{15}N, $^{13}C\alpha$, and $^{13}C_{\beta}$ resonance assignments plus six out of seven proline $^{13}C\alpha$ and $^{13}C_{\beta}$ resonances were assigned and 107 out of 125 $^{13}C'$ assignments were obtained for the N_{TAIL}–XD complex.

Titration of N_{TAIL} and XD

To gain further insight into the precise boundaries of the N_{TAIL} region involved in the interaction with XD, as well as into the dynamics of the binding reaction, NMR titration experiments were performed. In these experiments, ^{1}H-^{15}N HSQC spectra were collected on a 0.3 mM sample of N_{TAIL} in the presence of different concentrations of XD (Kay *et al*., 1992). The N_{TAIL} sample was uniformly labeled with ^{15}N and the XD sample was unlabeled. The first spectrum was collected on the free form of N_{TAIL} and then spectra were collected on N_{TAIL}-XD mixtures containing XD concentrations of 0.037, 0.075, 0.150, 0.3 and 0.6 mM. At low XD concentrations (0.037, 0.075, and 0.150 mM), most resonances in the HSQC experience no chemical shift changes (residues 401–474), some resonances undergo fast exchange and experience chemical shift changes with minimal line broadening (residues 475–482 and residues 507–525), and some resonances undergo intermediate exchange and experience significant line broadening (residues 483–506). For most resonances in this last category, the line broadening was so severe that a signal was no longer detectable. Exceptions include the resonances for residues 494 and 506, which will be discussed below. At high XD concentrations (0.3 and 0.6 mM), resonances for residues 492–501, and 503–506 reappeared at new positions, suggesting the formation of a stable complex. For all the affected resonances (residues 475–525), small chemical shift differences were observed when increasing the XD concentration from 0.3 to 0.6 mM, suggesting that binding is saturated.

The results for the N_{TAIL}/XD titration are summarized in Figures 5 and 6. Figure 5 shows the total chemical shift difference in Hz, from the ^{1}H-^{15}N HSQC spectra, for N_{TAIL} resonances at 0.0 and 0.6 mM concentrations of XD. Figure 5A shows the chemical shift differences using a scale that shows the largest values, while Figure 5B shows the chemical shift differences at a lower scale to highlight smaller, but significant differences. The combined digital resolution of the ^{1}H and ^{15}N dimensions in the HSQC experiment is 5 Hz and combined chemical shift differences greater than twice this value are considered significant. As shown in Figure 5, the most pronounced amide ^{1}H and ^{15}N chemical shift changes upon binding XD occur for N_{TAIL} residues 483–506. In addition, several residues in the Box3 region have chemical shift differences in the range of 20–30 Hz (Figure 5B).

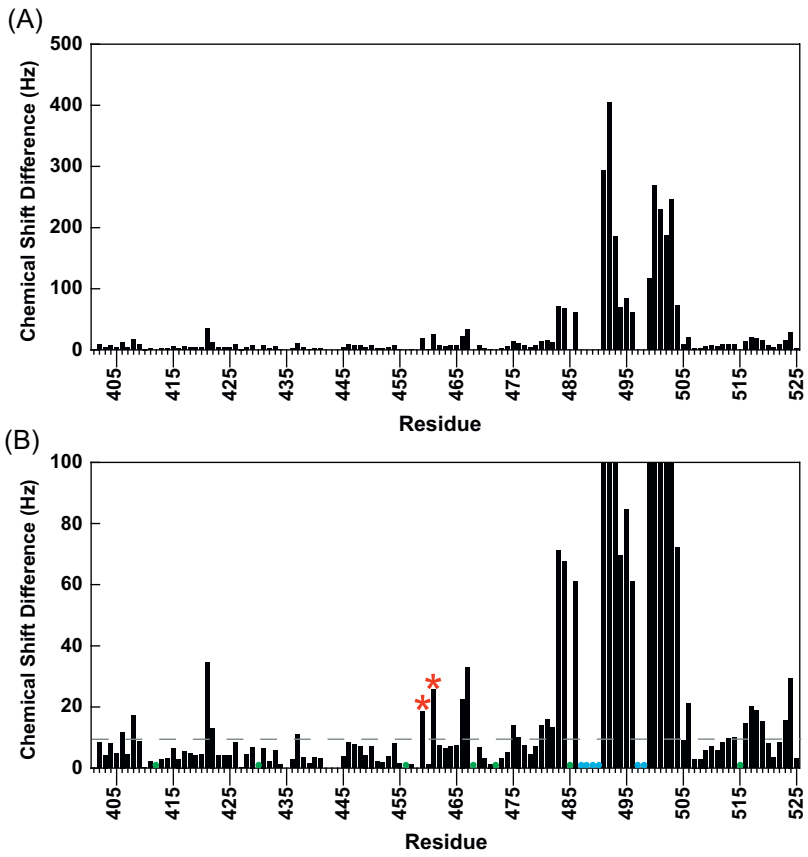

Figure 5. (A) Total ^{1}H and ^{15}N chemical shift differences in Hz for free and bound forms of N_{TAIL}. The N_{TAIL} concentration in both free and bound sample was 0.3 mM, while that of XD was 0.6 mM. In panel (B), the scale has been reduced so as to highlight smaller, yet significant, chemical shift changes. Dashed gray line is at two times the digital resolution (10 Hz). Stars show residues in the N-terminal half of N_{TAIL} that have resonance overlap with residues in the C-terminal half (where 459 overlaps with 518 and 461 overlaps with 516). Green dots correspond to proline residues and blue dots show the position of unassigned resonances in the N_{TAIL}/XD complex that probably have large chemical shifts changes.

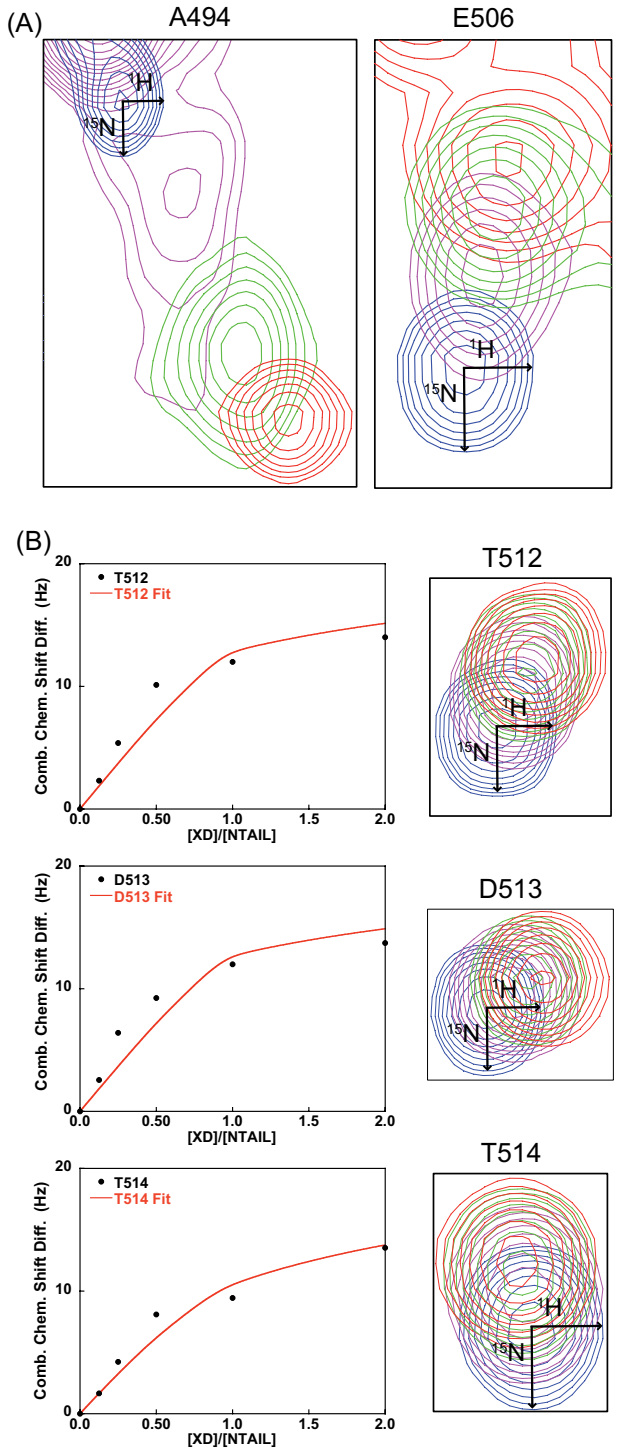

Figure 6. Resonance behavior and K_D estimates for the N_{TAIL}–XD complex. Resonances are shown for XD concentrations of 0.0 (blue), 0.075 (magenta), 0.15 (green), and 0.30 mM (red). N_{TAIL} concentration was held at 0.3 mM. Arrows show 10 Hz scale for ^{1}H and ^{15}N dimensions. (A) Resonances for residues A494 and E506 show evidence for intermediate exchange. (B) K_D estimates for residues that appear to be in fast exchange, T512-T514. The left panels show the combined chemical shift differences as a function of the [XD]/[N_{TAIL}] ratio. Data were fitted to a two-state model as described in Materials and Methods section.

Figure 6 shows the resonance behavior for several N_{TAIL} residues as well as attempts at estimating K_D values. Figure 6A shows resonances for residues A494 and E506 at XD concentrations of 0.0 (blue), 0.075 (magenta), 0.15 (green), and 0.30 (red) mM. These residues clearly show evidence for intermediate exchange during the titration. The resonances broaden at XD concentrations of 0.075 and 0.15 mM and become narrower at 0.30 mM. Note that A494 is the only residue from the 490–501 region whose resonance can be followed during the titration. The other resonances in this region are so broadened that they can no longer be detected in the middle of the titration. Many of these resonances reappear at XD concentrations of 0.30 and 0.60 mM.

Figure 6B shows the behavior of resonances that undergo fast exchange. In an attempt to achieve a more quantitative description of the binding between N_{TAIL} and XD, K_D values were tentatively estimated for these resonances. The left panels in Figure 6B show the combined chemical shift differences in Hz at each of the titration points plotted as a function of the XD/N_{TAIL} molar ratio. The red line shows the fit to the two-state model described in the Materials and Methods section. The K_D values for T512 and D513 are 11 and 12 μM, respectively, and the value for T514 is 50 μM. Note, however, that the standard deviation for all three of the fits is in the range of +/−30 μM. Interpretation of these results is presented in the discussion section.

Interaction with XD increases α-helical structure in N_{TAIL}

Unlabeled XD was also added to a 0.8 mM sample of N_{TAIL} uniformly labeled with ^{15}N and ^{13}C. Triple resonance experiments were performed on this sample, as well as on a sample of free N_{TAIL}, in order to make backbone resonance assignments. The details of data collection and analysis for the triple resonance experiments are described in Materials and Methods.

There is a well-established relationship between the chemical shifts of backbone nuclei and phi/psi dihedral angles, making this measurement a sensitive indicator of protein secondary structure (Wishart and Sykes, 1994a,b; Wishart and Nip, 1998; Schwarzinger *et al*., 2000; Schwarzinger *et al*., 2001; Wishart and Case, 2001). An important feature of particular relevance to intrinsically disordered proteins (IDPs) is that transient secondary structure can be detected by analyzing the backbone chemical shifts. A value, referred to as the secondary chemical shift ($\Delta\delta$), is determined by subtracting a random coil chemical shift standard from the chemical shift values of the ^{1}H, ^{15}N, $^{13}C\alpha$, $^{13}C_\beta$, and ^{13}CO resonances of the free and bound form of N_{TAIL}. Random coil chemical shift standard values were according to (Schwarzinger *et al*., 2000; Schwarzinger *et al*., 2001), except for Asp and Glu residues for which the random coil values were taken from (Wishart and Sykes, 1994a,b; Wishart and Nip, 1998; Wishart and Case, 2001). In both cases, values were corrected for nearest neighbor effects.

The $\Delta\delta$ values for $^{13}C\alpha$, and ^{13}CO of free and bound N_{TAIL} are plotted in Figure 7. For $^{13}C\alpha$ and ^{13}CO nuclei, positive $\Delta\delta$ values indicate the presence of helical structure. For $^{13}C\alpha$ and ^{13}CO nuclei, $\Delta\delta$ values greater than one indicate a fractional population of helical structure in the range of 50%. This is the case for residues 491–499 in free N_{TAIL}. The $^{13}C\alpha$ and ^{13}CO resonances for these same residues undergo positive shifts in their $\Delta\delta$ values in the presence of XD, indicating that the transient helical structure in free N_{TAIL} is stabilized in the N_{TAIL}-XD complex.

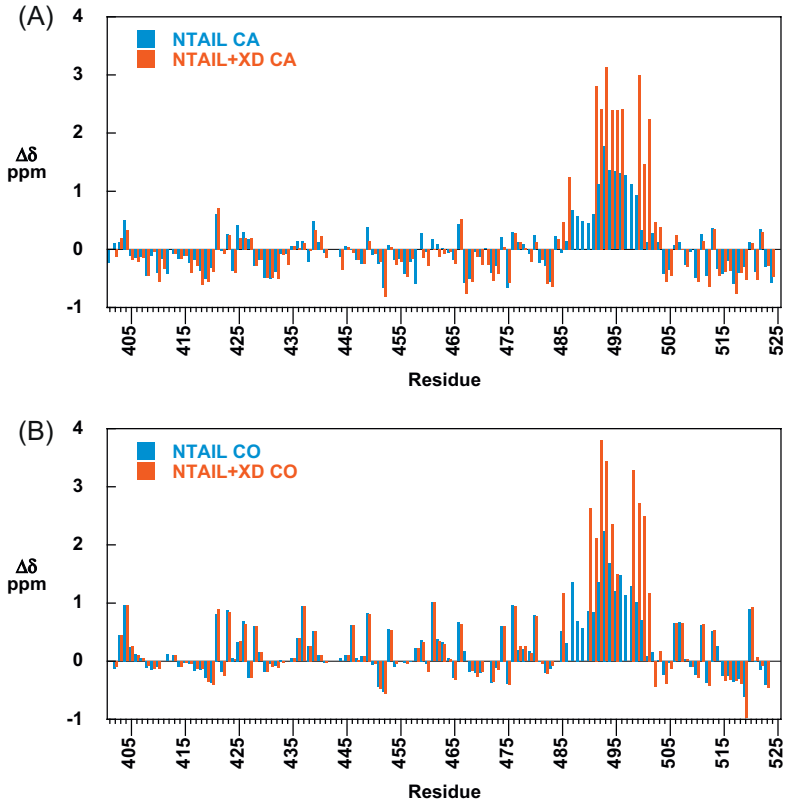

Figure 7. Secondary chemical shift differences ($\Delta\delta$) values for N_{TAIL} and the N_{TAIL}–XD complex with a respect to a random coil chemical shift standard (see text). The $\Delta\delta$ values are shown for (A) $^{13}C\alpha$ (CA) and (B) ^{13}CO (CO). Blue bars show the $\Delta\delta$ values for N_{TAIL} and red bars show the $\Delta\delta$ values for the N_{TAIL}–XD complex.

DISCUSSION

Solution structure of XD and comparison with other XD structures

The solution and crystal structures of MeV XD are very similar. In solution, although the structure is rather rigid, some residues located in the turn connecting the two last helices were found to be more flexible than the rest of the structure. We can speculate that this higher flexibility could favor the accommodation of N_{TAIL} in the hydrophobic cleft of XD, where binding of N_{TAIL} would take place through little structural rearrangement of XD and would imply only a minor rearrangement of $\alpha3$ paralleled by a reduction of the $\alpha2/\alpha3$ surface area. Notably, the higher flexibility of the loop connecting helices $\alpha2$ and $\alpha3$ is not a general feature of XD structures. Indeed in the crystal structure of MuV XD, this loop adopts the same conformation in the two molecules of the asymmetric unit and its B-factors are not significantly higher than the rest of the molecule (Kingston *et al*., 2008). Likewise, dynamics data from the SeV NMR structure indicate that the loop connecting helices $\alpha2$ and $\alpha3$ is less dynamic than its counterpart in MeV XD (Blanchard *et al*., 2004; Houben *et al*., 2007b).

The main striking difference between the SeV and MeV XD structures (irrespective of whether the structure has been solved by NMR or by X-ray crystallography) concerns the nature of the N_{TAIL}-binding interface. The N_{TAIL}-binding interface of MeV XD is prevalently apolar, whereas that of SeV XD is dominated by charged residues (Blanchard *et al*., 2004). The nucleocapsid-binding region within MuV XD has not been identified yet. However, sequence analysis of *Rubulavirus* P proteins pointed out a conservation of the C-terminal IIRSA motif, supporting helix $\alpha3$ as a plausible binding region (Kingston *et al*., 2008). Visual inspection of the MuV XD structure points out an abundance of hydrophobic residues within this region (see pdb code 3BBZ). The abundance of charged residues in the SeV XD nucleocapsid-binding interface is intriguing, since protein-protein interactions established by IDPs have been shown to rely more on hydrophobic–hydrophobic than on polar–polar contacts (Mészáros *et al*., 2007). Indeed, this is the case for MeV XD, whose prevalently apolar nature supports a mechanism where the burying of hydrophobic residues of N_{TAIL} at the hydrophobic cleft of XD would be the driving force in the N_{TAIL}-XD interaction (Johansson *et al*., 2003). On the other hand, and as already observed (Houben *et al*., 2007b), the prevalently charged nature of the N_{TAIL}-binding surface of SeV XD suggests a different binding mechanism in spite of a high degree of structural similarity. This binding diversity well explains the inability of MeV XD to restore replication in SeV XD-defective mutants (Curran and Kolakofsky, 1991), as well as the lack of interaction between SeV XD and MeV N_{TAIL} (Blackledge and Longhi, unpublished data).

Effect of XD on N_{TAIL} resonances

The addition of XD triggers no significant perturbation of the resonance frequencies of the 401–474 N_{TAIL} region, in agreement with previous BIAcore data that showed that removal of the 401–420 N_{TAIL} region has no impact on the XD binding reaction (Bourhis *et al*., 2005a), as well as with previous spectroscopic

studies indicating lack of XD effect on the mobility of spin labels grafted to positions 407 and 460 of N_{TAIL} (Morin *et al*., 2006; Belle *et al*., 2008). While previous studies showed that the 488–525 region of N_{TAIL} participates in the binding reaction (Bourhis *et al*., 2004; Bourhis *et al*., 2005a; Belle *et al*., 2008), the present study allowed us to further extend the region of interaction to residue 475, with the most pronounced XD effect concerning the 483–506 region. While this latter is in intermediate exchange, the upstream and downstream regions are in fast exchange. The intermediate nature of the exchange observed in the 483–506 region suggests that this is the primary binding site, in agreement with previous data (Bourhis *et al*., 2004; Bourhis *et al*., 2005a; Belle *et al*., 2008). Note that, for this region, peak broadening prevented meaningful estimations of dissociation constants towards XD. Strikingly, we obtained similar results upon addition of unlabeled N_{TAIL} to ^{15}N-labeled XD, and could estimate a K_D (20 μM) only for the binding reaction between XD and a Box2 peptide ($N^{487-507}$) (Bernard *et al*., 2009).

The pattern of chemical shift differences observed for the 477–505 region of N_{TAIL} in the presence of XD are similar to those observed with a labeled N_{TAIL} peptide encompassing this region titrated with XD (Kingston *et al*., 2004a). N_{TAIL} residues 507–525 are also affected by XD, as illustrated by the significant chemical shift changes that these resonances undergo in the presence of XD (see Figure 5), which is in agreement with previous studies (Bourhis *et al*., 2005a).

N_{TAIL} residues 507–525 are in fast exchange, thus allowing us to monitor chemical shift differences as a function of XD concentration. This led to K_D estimations ranging from 10 μM (T512 and D513) to 50 μM (T514), a value much higher than the one determined by previous surface plasmon resonance studies (80 nM) (Bourhis *et al*., 2005a). The poor quality of the fit, however, does not inspire a lot of confidence in the estimated K_D values. The poor fits of the titration data, and the observation that the chemical shift changes occurring at early titration points (when N_{TAIL} is in excess) are larger than expected, suggest that another process, in addition to binding, is contributing to the magnitude of the chemical shift changes. Since N_{TAIL} folds upon binding to XD, the observed titration behavior may be accounted for by assuming the existence of a binding intermediate in the form of a weak, non-specific encounter complex, where this can be considered as an ensemble of short-lived, low free-energy states.

A non-two-state binding process between N_{TAIL} and XD is in contrast to a previous study of the N_{TAIL}–XD interaction that was performed using XD and an N_{TAIL} peptide encompassing residues 477–505 (Kingston *et al*., 2004a). This previous study monitored the resonances of XD and provided evidence for two-state behavior, with the K_D estimated to be 13 μM (Kingston *et al*., 2004a).

That different titration behaviors are observed depending on whether the monitored resonances are those of the folded or of the unfolded partner has already been reported for the p53TAD/RPA70 complex, and has been assumed to reflect the presence of a folding intermediate (e.g. encounter complex) for p53TAD (Vise *et al*., 2005). The fact that this transient state is only observed when the resonances of the disordered partner are monitored is simply due to the way NMR titrations are performed. When the resonances of the disordered partner are monitored, the protein is in excess at the beginning of the titration, which provides an opportunity for the intermediate to accumulate and be detected. When the resonances of the ordered protein are monitored, the disordered partner is only in excess at the end of the titration. At this point, the binding is approaching saturation and the intermediate cannot be detected. Another plausible explanation of the N_{TAIL} resonance behavior could be the presence of some non-specific effect due to the presence of the N-terminal and/or C-terminal unfolded regions.

Pre-formed α-helical structure within N_{TAIL}

The changes in Δδ values observed for the $^{13}C\alpha$ and ^{13}CO nuclei support the existence of an α-helical conformation within residues 491–499 in the free form of N_{TAIL}. Although previous titration studies that were performed using a labeled 477–505 N_{TAIL} peptide had already indicated the presence of a loosely structured state mimicking the bound conformation within the 487–503 region in the absence of the partner (Kingston *et al*., 2004a), the present study allowed us to address the possible effect of the disordered flanking regions on the stabilization of the partly populated α-helical region. The results herein presented support lack of α-helical stabilization by the flanking disordered N_{TAIL} regions, as judged based on the comparison of Δδ values observed for the $^{13}C\alpha$ nuclei of full length N_{TAIL} and of the $N^{477-505}$ peptide. They also confirm and extend previous EPR studies showing that the 488–502 region of N_{TAIL} is transiently populated as an α-helix in the absence of the partner (Belle *et al*., 2008). Indeed, previous EPR studies only probed the 488–522 region, thereby providing no information on upstream residues. Since the experimental design of the present study allowed all N_{TAIL} sites to be probed, the results presented here provide the first demonstration of the precise boundaries of α-helical sampling within N_{TAIL}.

XD-induced structural transitions within N_{TAIL}

The changes in Δδ values observed for the $^{13}C\alpha$ and ^{13}CO nuclei, between the free and bound form of N_{TAIL}, provides clear evidence for a gain of α-helical structure for residues 490–504. Conversely, no changes in secondary structure are observed for the downstream region, although significant chemical shift changes are observed in the ^{1}H-^{15}N HSQC titration experiments. In particular, the values for the chemical shift differences go down for residues 507–514 and then go back up for the Box3 residues. Lack of a regular XD-induced structural transition for N_{TAIL} residues 505–525 is in agreement with previous NMR and EPR studies (Bourhis *et al*., 2005a; Belle *et al*., 2008).

CONCLUSIONS

Along with previous studies, the data presented in this report support a model of the N_{TAIL}–XD interaction where Box2 is the primary binding site and the binding mechanism involves both conformer selection and non-specific encounter complex formation. The presence of a transient helical segment in free N_{TAIL} supports the conformer selection model and suggests a sub-population of pre-formed helices are available for specific binding to XD. A path for binding could also be available through the formation of a non-specific encounter complex. In the extreme case of this model, a form of N_{TAIL} with little or no helical content will form a weak encounter complex with XD, which is followed by the folding of the N_{TAIL} helical segment. This possibility is suggested from the resonance lineshape behavior of the N_{TAIL}-XD titration data. These two mechanisms are not

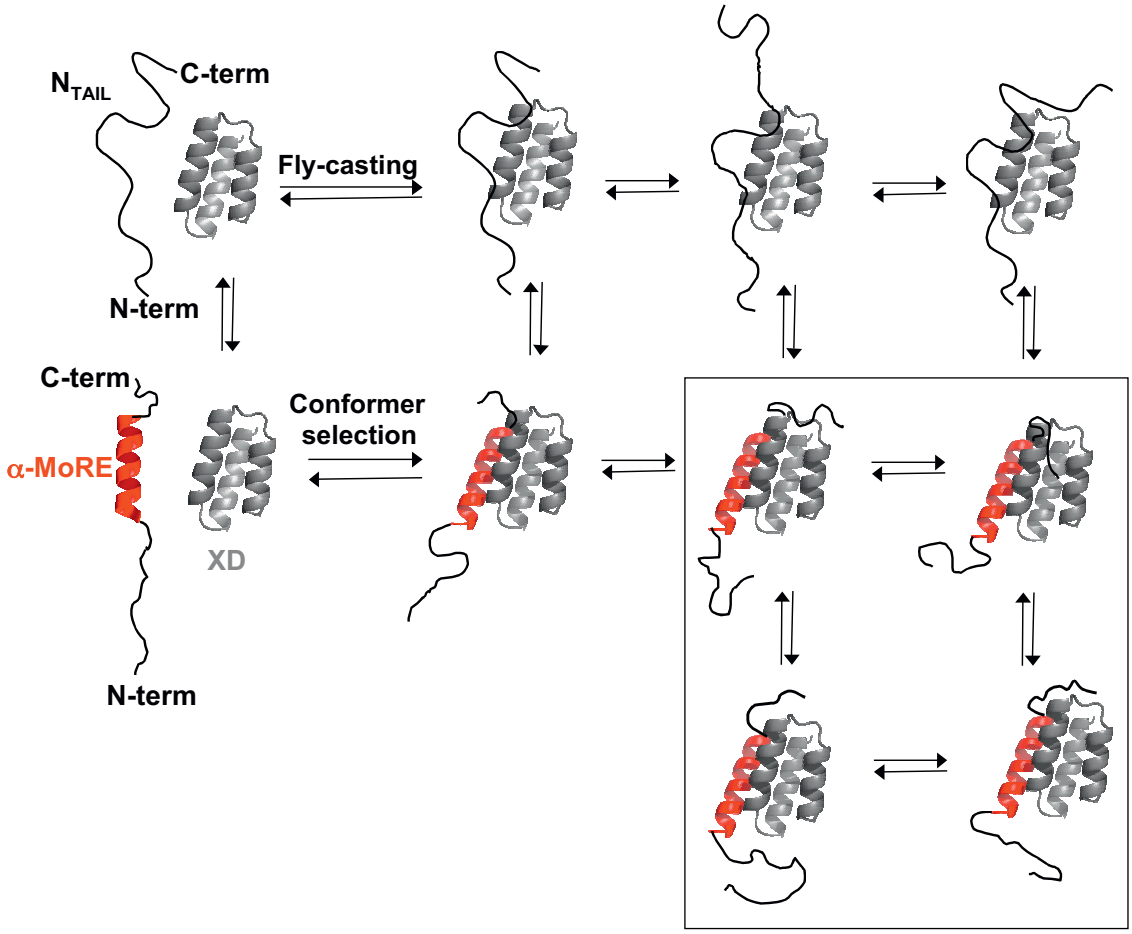

Figure 8. Model for N_{TAIL}–XD complex formation that utilizes both conformer selection and non-specific encounter complex formation. The red helix, corresponding to the primary binding site for XD, occurs in roughly 50% of the population of N_{TAIL} molecules, where it encompasses residues 491–499. In the non-specific binding model, a weak encounter complex may also form between N_{TAIL} and XD. This encounter complex is converted to a tightly bound complex by the folding of residues 490–504. It is unclear if this folding occurs during the lifetime of the encounter complex. In the conformer selection model, the preformed helix interacts with XD to form a tightly bound complex. In both cases, following α-helical folding of Box2, Box3 becomes more rigid. The four conformers that are framed schematically represent the final stage in complex formation, which consists of an ensemble of conformers in which Box3 has a reduced conformational freedom that may favor the establishment of weak, non-specific contacts with XD.

mutually exclusive and fit into a single thermodynamic cycle that is illustrated in Figure 8.

It remains unclear exactly what role Box3 plays in the interaction with XD. In agreement with previous spectroscopic data (Bourhis *et al*., 2005a; Belle *et al*., 2008), the present study clearly shows no evidence of structure formation within Box3, as judged based on free and bound $\Delta\delta$ values for CA and CO. Interestingly, this observation is in agreement with recent studies by the group of Sigalov who also showed that the intrinsically disordered cytoplasmic domain of the T cell receptor zeta subunit does not undergo a transition between a disordered and an ordered state upon dimerization (Sigalov *et al*., 2007; Sigalov *et al*., 2008). Yet, previous SPR studies clearly indicate that eliminating Box3 reduces the affinity between N_{TAIL} and XD (Bourhis *et al*., 2005a).

Although Box3 does not undergo any regular structural transition, the chemical shift changes observed for Box3 residues in the ^{1}H-^{15}N HSQC spectrum of the N_{TAIL}–XD complex do indicate a change in the local electronic environment of these residues. We think that it is unlikely that Box3 stabilizes the α-helix formed by N_{TAIL} residues 490–504, since (i) $\Delta\delta$ values observed for the $^{13}C\alpha$ nuclei of full length N_{TAIL} and a peptide corresponding to residues 477–505 are very similar, and (ii) analysis of ^{15}N 3D-NOESY of free and bound N_{TAIL} showed no evidence of an interaction between Box2 and Box3 (data not shown). On the other hand, previous studies did not detect any direct contacts between XD and Box3 (Belle *et al*., 2008; Bernard *et al*., 2009), although those studies did show an increase in the rigidity of this region (Belle *et al*., 2008). Notably, in these latter studies TFE was shown to induce a reduction in Box3 mobility similar to that triggered by XD, thus ruling out the possibility that the increased rigidity of Box3 may arise from a steric hindrance brought about by the presence of XD (Belle *et al*., 2008).

Taken together, these data suggest that the mobility of Box3 is restricted in the presence of XD probably as a result of α-helical folding of the neighboring Box2 region. The reduced conformational sampling of Box3 might favor the establishment of weak, non-specific contacts with XD that may contribute to stabilizing the N_{TAIL}-XD complex (see Figure 8).

Acknowledgements

This work was carried out with the financial support of the Agence Nationale de la Recherche, specific program "Microbiologie et Immunologie", ANR-05-MIIM-035-02, of the National Institute of Neurological Disorders and Stroke, specific program R01 NS031693-11A2, and of the CNRS. GWD is funded by the American Cancer Society (RSG-07-289-01-GMC) and the National Science Foundation (0744839). The authors wish to thank Elodie Liquière for technical help in producing and purifying the protein samples. MRJ received support form EMBO and Lundbeckfonden.

REFERENCES

Albertini AA, Wernimont AK, Muziol T, Ravelli RB, Clapier CR, Schoehn G, Weissenhorn W, Ruigrok RW. 2006. Crystal structure of the rabies virus nucleoprotein-RNA complex. *Science* **313**: 360–363.

Belle V, Rouger S, Costanzo S, Liquiere E, Strancar J, Guigliarelli B, Fournel A, Longhi S. 2008. Mapping alpha-helical induced folding within the intrinsically disordered C-terminal domain of the measles virus nucleoprotein by site-directed spin-labeling EPR spectroscopy. *Proteins* **73**: 973–988.

Bernado P, Blanchard L, Timmins P, Marion D, Ruigrok RW, Blackledge M. 2005. A structural model for unfolded proteins from residual dipolar couplings and small-angle X-ray scattering. *Proc. Natl Acad. Sci. USA* **102**: 17002–17007.

Bernard C, Gely S, Bourhis JM, Morelli X, Longhi S, Darbon H. 2009. Interaction between the C-terminal domains of N and P proteins of measles virus investigated by NMR. *FEBS Lett.* **583**: 1084–1089.

Blanchard L, Tarbouriech N, Blackledge M, Timmins P, Burmeister WP, Ruigrok RW, Marion D. 2004. Structure and dynamics of the nucleocapsid-binding domain of the Sendai virus phosphoprotein in solution. *Virology* **319**: 201–211.

Bourhis J, Johansson K, Receveur-Bréchot V, Oldfield CJ, Dunker AK, Canard B, Longhi S. 2004. The C-terminal domain of measles virus nucleoprotein belongs to the classof intrinsically disordered proteins that fold upon binding to their pohysiological partner. *Virus Res.* **99**: 157–167.

Bourhis JM, Receveur-Bréchot V, Oglesbee M, Zhang X, Buccellato M, Darbon H, Canard B, Finet S, Longhi S. 2005a. The intrinsically disordered C-terminal domain of the measles virus nucleoprotein interacts with the C-terminal domain of the phosphoprotein via two distinct sites and remains predominantly unfolded. *Protein Sci.* **14**: 1975–1992.

Bourhis JM, Canard B, Longhi S. 2005b. Désordre structural au sein du complexe réplicatif du virus de la rougeole: implications fonctionnelles. *Virologie* **9**: 367–383.

Bourhis JM, Canard B, Longhi S. 2006. Structural disorder within the replicative complex of measles virus: functional implications. *Virology* **344**: 94–110.

Bourhis JM, Longhi S. 2007. Measles virus nucleoprotein: structural organization and functional role of the intrinsically disordered C-terminal domain. In Measles Virus Nucleoprotein, Longhi S (ed.). Nova Publishers Inc.: Hauppage, NY; 1–35.

Curran JA, Kolakofsky D. 1991. Rescue of a Sendai virus DI genome by other parainfluenza viruses: implications for genome replication. *Virology* **182**: 168–176.

Delaglio F, Grzesiek S, Vuister GW, Zhu G, Pfeifer J, Bax A. 1995. NMRPipe: a multidimensional spectral processing system based on UNIX pipes. *J. Biomol. NMR* **6**: 277–293.

DeLano WL. 2002. The PyMOL molecular graphics system proteins: structure. *Funct. Bioinform.* **30**: 442–454.

Farrow NA, Muhandiram R, Singer AU, Pascal SM, Kay CM, Gish G, Shoelson SE, Pawson T, Forman-Kay JD, Kay LE. 1994. Backbone dynamics of a free and phosphopeptide-complexed Src homology 2 domain studied by 15N NMR relaxation. *Biochemistry* **33**: 5984–6003.

Fuxreiter M, Tompa P, Simon I. 2007. Local structural disorder imparts plasticity on linear motifs. *Bioinformatics* **23**: 950–956.

Goddard TD, Kneller DG. 2003. University of California.

Green TJ, Zhang X, Wertz GW, Luo M. 2006. Structure of the vesicular stomatitis virus nucleoprotein-RNA complex. *Science* **313**: 357–360.

Houben K, Marion D, Tarbouriech N, Ruigrok RW, Blanchard L. 2007a. Interaction of the C-terminal domains of sendai virus N and P proteins: comparison of polymerase-nucleocapsid interactions within the paramyxovirus family. *J. Virol.* **81**: 6807–6816.

Houben K, Blanchard L, Blackledge M, Marion D. 2007b. Intrinsic dynamics of the partly unstructured PX domain from the Sendai virus RNA polymerase cofactor P. *Biophys. J.* **93**: 2830–2844.

Jensen MR, Houben K, Lescop E, Blanchard L, Ruigrok RW, Blackledge M. 2008. Quantitative conformational analysis of partially folded proteins from residual dipolar couplings: application to the molecular recognition element of Sendai virus nucleoprotein. *J. Am. Chem. Soc.* **130**: 8055–8061.

Johansson K, Bourhis JM, Campanacci V, Cambillau C, Canard B, Longhi S. 2003. Crystal structure of the measles virus phosphoprotein domain responsible for the induced folding of the C-terminal domain of the nucleoprotein. *J. Biol. Chem.* **278**: 44567–44573.

Johnson BA, Blevins RA. 1994. NMRView: a computer program for the visualization and analysis of NMR data. *J. Biomol. NMR* **4**: 603–614.

Jung YS, Zweckstetter M. 2004. Mars – robust automatic backbone assignment of proteins. *J. Biomol. NMR* **30**: 11–23.

Karlin D, Ferron F, Canard B, Longhi S. 2003. Structural disorder and modular organization in Paramyxovirinae N and P. *J. Gen. Virol.* **84**: 3239–3252.

Karlin D, Longhi S, Receveur V, Canard B. 2002a. The N-terminal domain of the phosphoprotein of morbilliviruses belongs to the natively unfolded class of proteins. *Virology* **296**: 251–262.

Karlin D, Longhi S, Canard B. 2002b. Substitution of two residues in the measles virus nucleoprotein results in an impaired self-association. *Virology* **302**: 420–432.

Kay LE, Keifer P, Saarinen T. 1992. Pure absorption gradient enhanced heteronuclear single quantum correlation spectroscopy with improved sensitivity. *J. Am. Chem. Soc.* **114**: 10663.

Kingston RL, Gay LS, Baase WS, Matthews BW. 2008. Structure of the nucleocapsid-binding domain from the mumps virus polymerase; an example of protein folding induced by crystallization. *J. Mol. Biol.* **379**: 719–71931.

Kingston RL, Hamel DJ, Gay LS, Dahlquist FW, Matthews BW. 2004a. Structural basis for the attachment of a paramyxoviral polymerase to its template. *Proc. Natl Acad. Sci. USA* **101**: 8301–8306.

Kingston RL, Walter AB, Gay LS. 2004b. Characterization of nucleocapsid binding by the measles and the mumps virus phosphoprotein. *J. Virol.* **78**: 8615–8629.

Laskowski RA, MacArthur MW, Moss DM, Thornton JM. 1993. A program to check the stereochemical quality of protein structures. *J. Appl. Cryst.* **26**: 283–291.

Lescop E, Schanda P, Brutscher B. 2007. A set of BEST triple-resonance experiments for time-optimized protein resonance assignment. *J. Magn. Reson.* **187**: 163–169.

Linge JP, Habeck M, Rieping W, Nilges M. 2003. ARIA: Automated NOE assignment and NMR structure calculation. *Bioinformatics* **19**: 315–316.

Longhi S, Canard B. 1999. Mécanismes de transcription et de réplication des *Paramyxoviridae*. *Virologie* **3**: 227–240.

Longhi S, Receveur-Brechot V, Karlin D, Johansson K, Darbon H, Bhella D, Yeo R, Finet S, Canard B. 2003. The C-terminal domain of the measles virus nucleoprotein is intrinsically disordered and folds upon binding to the C-terminal moiety of the phosphoprotein. *J. Biol. Chem.* **278**: 18638–18648.

Longhi S. 2009. Nucleocapsid Structure and Function. *Curr. Top. Microbiol. Immunol.* **329**: 103–128.

Macura S, Ernst RR. 1980. Elucidation of cross relaxation in liquids by two-dimensional N.M.R. spectroscopy. *Mol. Phys.* **41**: 95–117.

Meszaros B, Tompa P, Simon I, Dosztanyi Z. 2007. Molecular principles of the interactions of disordered proteins. *J. Mol. Biol.* **372**: 549–561.

Mohan A, Oldfield CJ, Radivojac P, Vacic V, Cortese MS, Dunker AK, Uversky VN. 2006. Analysis of Molecular Recognition Features (MoRFs). *J. Mol. Biol.* **362**: 1043–1059.

Morin B, Bourhis JM, Belle V, Woudstra M, Carrière F, BGuigliarelli B, Fournel A, LonghiS., 2006. Assessing induced folding of an intrinsically disordered protein by site-directed spin-labeling EPR spectroscopy. *J. Phys. Chem. B* **110**: 20596–20608.

Muhandiram DR, Kay LE. 1994. Gradient-enhanced triple-resonance three-dimensional NMR Experiments with improved sensitivity. *J. Magn. Reson. B* **3**: 203–216.

Mulder FA, Schipper D, Bott R, Boelens R. 1999. Altered flexibility in the substrate-binding site of related native and engineered high-alkaline Bacillus subtilisins. *J. Mol. Biol.* **292**: 111–123.

Oldfield CJ, Cheng Y, Cortese MS, Romero P, Uversky VN, Dunker AK. 2005. Coupled folding and binding with alpha-helix-forming molecular recognition elements. *Biochemistry* **44**: 12454–12470.

Schanda P, Van Melckebeke H, Brutscher B. 2006. Speeding up three-dimensional protein NMR experiments to a few minutes. *J. Am. Chem. Soc.* **128**: 9042–9043.

Schwarzinger S, Kroon GJ, Foss TR, Chung J, Wright PE, Dyson HJ. 2001. Sequence-dependent correction of random coil NMR chemical shifts. *J. Am. Chem. Soc.* **123**: 2970–2978.

Schwarzinger S, Kroon GJ, Foss TR, Wright PE, Dyson HJ. 2000. Random coil chemical shifts in acidic 8 M urea: implementation of random coil shift data in NMRView. *J. Biomol. NMR* **18**: 43–48.

Sigalov AB, Zhuravleva AV, Orekhov VY. 2007. Binding of intrinsically disordered proteins is not necessarily accompanied by a structural transition to a folded form. *Biochimie* **89**: 419–421.

Sigalov AB, Kim WM, Saline M, Stern LJ. 2008. The intrinsically disordered cytoplasmic domain of the T cell receptor zeta chain binds to the nef protein of simian immunodeficiency virus without a disorder-to-order transition. *Biochemistry* **47**: 12942–12944.

Tarbouriech N, Curran J, Ruigrok RW, Burmeister WP. 2000. Tetrameric coiled coil domain of Sendai virus phosphoprotein. *Nat. Struct. Biol.* **7**: 777–781.

Vacic V, Oldfield CJ, Mohan A, Radivojac P, Cortese MS, Uversky VN, Dunker AK. 2007. Characterization of molecular recognition features, MoRFs, and their binding partners. *J. Proteome Res.* **6**: 2351–2366.

Vise PD, Baral B, Latos AJ, Daughdrill GW. 2005. NMR chemical shift and relaxation measurements provide evidence for the coupled folding and binding of the p53 transactivation domain. *Nucleic Acids Res.* **33**: 2061–2077.

Wishart DS, Sykes BD. 1994a. The 13C chemical-shift index: a simple method for the identification of protein secondary structure using 13C chemical-shift data. *J. Biomol. NMR* **4**: 171–180.

Wishart DS, Case DA. 2001. Use of chemical shifts in macromolecular structure determination. *Methods Enzymol.* **338**: 3–34.

Wishart DS, Sykes BD. 1994b. Chemical shifts as a tool for structure determination. *Methods Enzymol.* **239**: 363–392.

Wishart DS, Nip AM. 1998. Protein chemical shift analysis: a practical guide. *Biochem. Cell. Biol.* **76**: 153–163.

Wittekind M, Mueller L. 1993. HNCACB, a high-sensitivity 3D NMR experiment to correlate amide-proton and nitrogen resonances with the alpha- and beta-carbon resonances in proteins. *J. Magn. Reson. B* **2**: 201–205.

